Large Eddy Simulations of Flow Over a Wall-Mounted Cube at $Re_h = 40,000$

Vedant Puri[1] and Ramesh Balakrishnan[1]

[1]Computational Science Division, Argonne National Laboratory, Lemont, IL-60439

July 14, 2020

Abstract

During the third quarter (Q3), the Argonne team has made progress towards comparing our Nek5000 wall modeled large eddy simulations (WMLES) of the flow over a wall mounted cube (WMC), at two different orientations to the incoming wind vector, and comparing the results of our simulations with the experimental results of Snyder *et al.*. As shown by our comparisons, our results compare favorably with the experimental results and upholds our conjectures regarding the *insensitivity* of the flow characteristics downstream of the cube, to the upstream turbulence intensity of the incoming flow. This, together with our earlier observations (noted in the Q2 report) about the insensitivity of the downstream flow to the Reynolds number (Re_h), are factors that will inform the development of Reynolds Averaged Navier–Stokes (RANS) and other lower order sub-grid models.

1 Introduction

Large Eddy Simulations of flow past a wall-mounted cube at Reynolds number $Re_h = 40,000$ have been conducted using the spectral-element computational fluid dynamics code Nek5000. Two geometries are considered: the cube oriented at a 45° (WMC45) and a 90° (WMC90) angle with respect to the inflow direction. The incidence of flow onto a bluff body creates regions of separation and recirculation, followed by a wake with recovering velocity deficit. We compare the results from cases WMC45, and WMC90 with data collected from wind-tunnel experiments described in Snyder, 1994 [1]. Future work involves considering two different mean-shear profiles: Blasius boundary layer with δ_{99} at a quarter of the cube height; and Blasius boundary layer with δ_{99} at twice the cube height.

2 Case Overview and Setup

A uniform cube of side h is mounted on a smooth box $[-10h, 25h] \times [0, 5h] \times [-5h, 5h]$. We refer to $\hat{\boldsymbol{x}}$, $\hat{\boldsymbol{y}}$, $\hat{\boldsymbol{z}}$ as the streamwise, "ground"-normal (to the box), and spanwise directions. The base of the cube is centred at the origin. In case WMC90, the incident surface of the cube is perpendicular to $\hat{\boldsymbol{x}}$. In case WMC45, the cube is rotated 45° about $\hat{\boldsymbol{z}}$ such that the incident face(s) make an angle of 45° with

$\hat{\boldsymbol{x}}$. The computational domain is defined as the volume of the box from which the cube is subtracted. The streamwise extent of the domain is $9.5h$ upstream of the cube, to allow the flow to develop and adjust to the presence of the obstacle, and $24.5h$ downstream to capture the wake of the flow in the far field.

Boundary conditions applied to the computational domain are as follows: 'no-slip' on the ground ($y = 0$), and on the surface of the cube; Dirichlet 'inflow', and Neumann 'outflow' on $x = -10h,\ 25h$ respectively; 'slip' on the top of the box $y = 5h$; and 'periodic' in the spanwise direction (on planes $z = \pm 5h$). Periodicity effectively simulates an infinitely wide array of cubes separated by a spanwise distance of $10h$. The slip condition is not representative of an obstacle in a channel, much less the atmospheric boundary layer, and mostly closely represents simulation up to the momentum displacement thickness of a gradually slanted wall (provided wake turbulence decays to zero by the top boundary condition).

We consider a laminar power-law inflow profile matching the experimental results collected by [1]. The Reynolds number of the flow with respect to the cube height, h, and characteristic streamwise velocity, U, is set to be $Re_h = \dfrac{Uh}{\nu} = 40,000$. To match the experimental conditions of [1], the characteristic velocity for the case with 'Snyder' inflow is $U = v_x(y = h)$, i.e. the velocity at cube height. Figure 1 shows the the flow profiles next to the wall-mounted cube.

We use the spectral-element CFD code Nek5000[4] for its excellent scalability. In the spectral element method, in Nek5000, teh solution field is represented, locally, in each spectral element, by Gauss-Lobatto-Legendre polynomials, while maintaining C_0 continuity over element boundaries. The code numerically solves the Navier-Stokes equation (Eq. 1) using a second order Backward Difference Formula for time-stepping with explicit treatment of the convection term $(\boldsymbol{u}\cdot\boldsymbol{\nabla})\boldsymbol{u}$, and implicit treatment of the diffusion term $\nabla^2\boldsymbol{u}$. We note that the numerical simulations described in this study are implicit Large Eddy Simulations. That is, no explicit sub-grid stress model is employed in the numerical simulations. Instead, the Fischer-Mullen filter [5], which contributes to the stability of the spectral method, at high Reynolds numbers, also serves as a sub-grid model for the unresolved length scales.

$$\begin{aligned} \rho(\partial_t + \boldsymbol{v}\cdot\boldsymbol{\nabla})\boldsymbol{v} &= -\boldsymbol{\nabla}p + \mu\nabla^2\boldsymbol{v} + \rho\boldsymbol{f} \\ \boldsymbol{\nabla}\cdot\boldsymbol{v} &= 0 \end{aligned} \tag{1}$$

The computational domains for WMC45, and WMC90 are tessellated with $376K$, and $300K$ spectral elements respectively. The surface topologies of the element meshes, as constructed in Gmsh[2], are presented in Figure 2. Each mesh is composed of a finely resolved region focusing on the cube, and a coarsely resolved far field region. The surface of the cube is spanned by 30 spectral elements in the lateral directions. The ground normal direction is covered by 29 spectral elements with an expansion factor of 1.1. Each spectral element is spanned by seventh-order tensor-product polynomials resulting 512 grid-points per spectral element.

Due to limited computational resources and the intention of this group to conduct future simulations outlined in § 4, the resolution of the meshes correspond to that of a coarse LES. The flow is allowed to develop for a single flow-through time, i.e. time taken for a fluid element advected by the characteristic velocity to traverse the streamwise length of the domain. That is $35h/U$ Statistics are computed for approximately 20 convective time units, h/U, a fraction of the recommended 100 convective time units for bluff body flows[3].

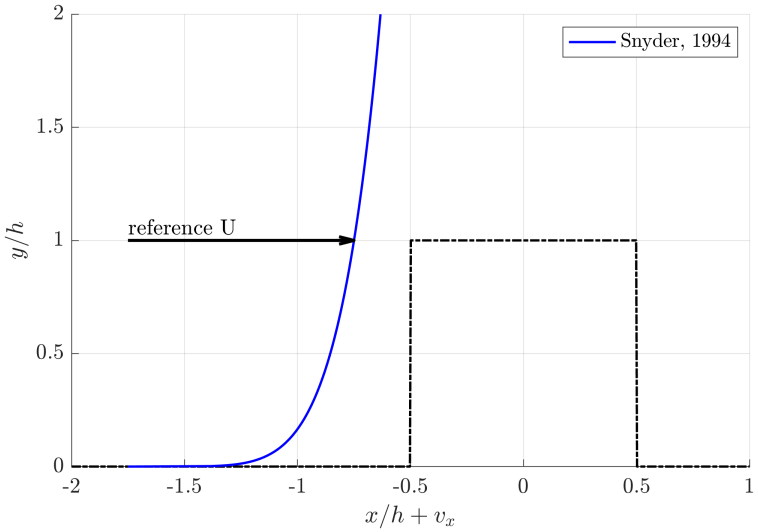

Figure 1: Inflow velocity profile matching the experimental results of Snyder, 1994.

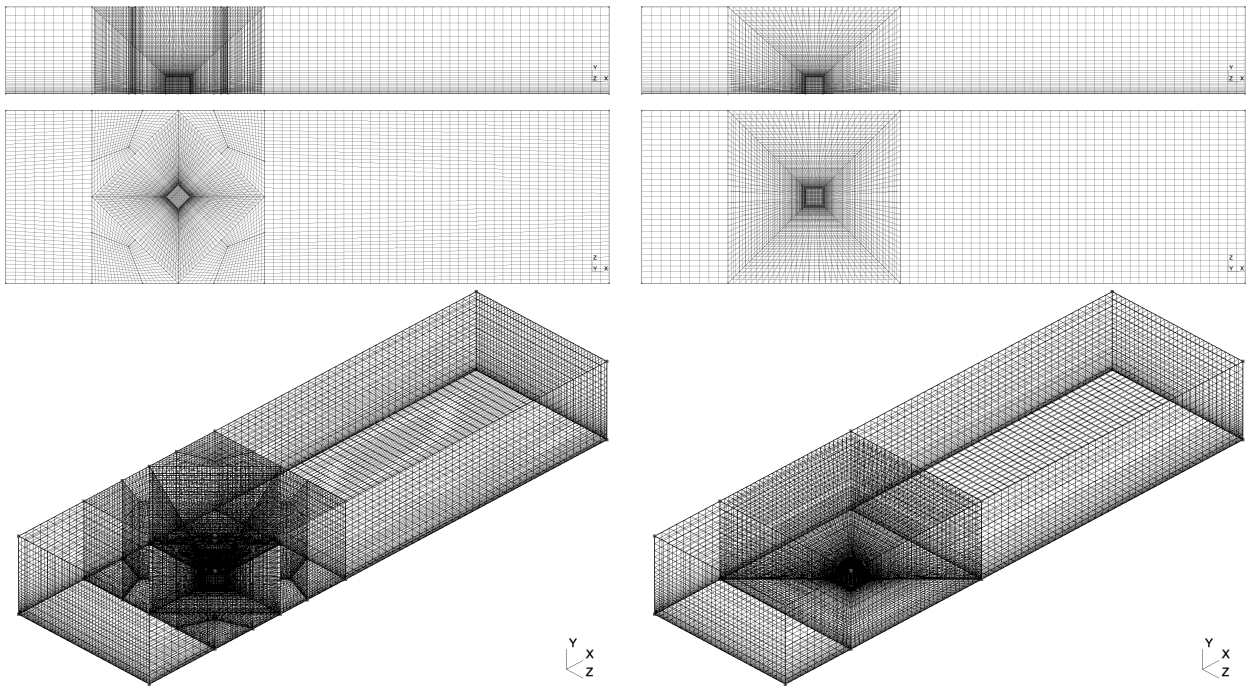

(a) WMC45 (b) WMC90

Figure 2: Mesh Surface Topologies - side view, top view, isometric view

While the laminar inlet velocity profile and smooth walls are not representative of true obstacle flows in an atmospheric boundary layer, the simulation is still representative of characteristics of interest and may be used to guide and progress to modeled turbulence methods which will be computationally feasible. The decision to use a laminar inflow velocity profile stems from our observations of the DNS and WRLES solution fields of flow over a unit cube at $Re_h = 3900$ and $Re_h = 20,000$ respectively, where it was seen that the flow field downstream of the cube is insensitive to the Reynolds number, and the inflow turbulence intensity.

3 Results

We solve for the flow in neutral conditions, i.e. free of any temperature effects, for the cases WMC45, and WMC90. To assess the accuracy of the computations, mean streamwise velocity, v_x, profiles are compared against the [1] dataset on the vertical centerline plane, $z = 0$, and on the 'ground' plane $y = 0.1h$. The profiles are plotted in Figure 3 and Figure 4 for WMC45 and WMC90 respectively. Similarly, Turbulent kinetic energy (TKE), k profiles are compared on the same planes in Figure 5 and Figure 6 for WMC45 and WMC90 respectively. Due to experimental limitations, was unable to measure flow velocity normal to the plane of measurement. Therefore, k is approximated as $3/2(v_x^2 + v_y^2)$ on the centerline plane, and as $3/2(v_x^2 + v_z^2)$ on the ground plane.

The WMC45 and WMC90 simulations successfully capture the mean shear profile and turbulent kinetic energy near the cube, and in the far-field. Despite the coarse resolution and short time-span for statistics collection, the use of a laminar inflow profile, and no wall functions to model the roughness of the ground (on which the cube was placed), the comparisons between our simulation results and the EPA (Snyder) experimental data is favorable.

Pertinent features of the flow relevant to the placement of wind turbines near buildings are the following: extent and intensity of the velocity-deficit region in the wake of the cube; and intensity of flow speedup above the building. Wind turbines benefit from a flow 'speedup' and may produce more energy. However, the flow in the wake of the cube is turbulent and large variations in flow profile may cause early turbine failure due to rotor wear and tear. To assess both flow speedup and velocity fluctuations, we plot streamwise velocity speedup, and turbulent kinetic energy along $\hat{\boldsymbol{x}}$ at multiple heights above the cube in Figure 7 and Figure 8.

4 Continuing Work

In our continuing work, we will be assess the effects of turbulence intensity, and surface roughness, together with varying inflow mean shear, on the flow field downstream of the cube.

5 Acknowledgements

We gratefully acknowledge use of the Bebop cluster in the Laboratory Computing Resource Center at Argonne National Laboratory. This research used resources of the Argonne Leadership Computing

Facility, which is a DOE Office of Science User Facility supported under Contract DE-AC02-06CH11357.

6 References

[1] Snyder, W. AND R.E. Lawson, Jr. WIND-TUNNEL MEASUREMENTS OF FLOW FIELDS IN THE VICINITY OF BUILDINGS. U.S. Environmental Protection Agency, Washington, D.C., EPA/600/A-93/230 (NTIS PB93236594).

[2] C. Geuzaine and J.-F. Remacle, Gmsh: a three-dimensional finite element mesh generator with built-in pre- and post-processing facilities. International Journal for Numerical Methods in Engineering, Volume 79, Issue 11, pages 1309-1331, 2009.

[3] W. Rodi, J. H. Ferziger, M. Breuer, and M. Pourquie, "Status of large eddy simulation: Results of a workshop," Transactions of the ASME, vol. 119, pp. 248–262, 1997.

[4] Argonne National Laboratory, Illinois., *Nek5000*, version 17.0. [Online]. Available: `https://nek5000.mcs.anl.gov`.

[5] J. S. Mullen and P. F. Fischer, "Filtering techniques for complex geometry fluid flows," *Communications in Numerical Methods in Engineering*, vol. 15, no. 1, pp. 9–18, 1999.

Appendix

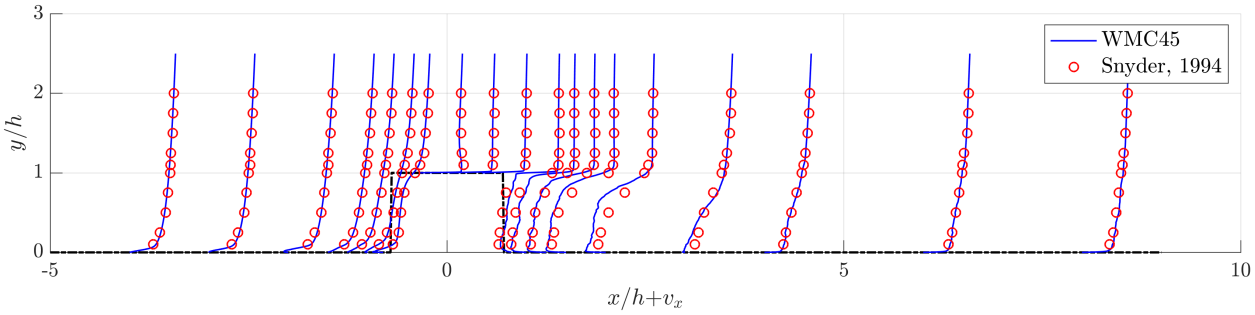

(a) Centerline plane, $z = 0$

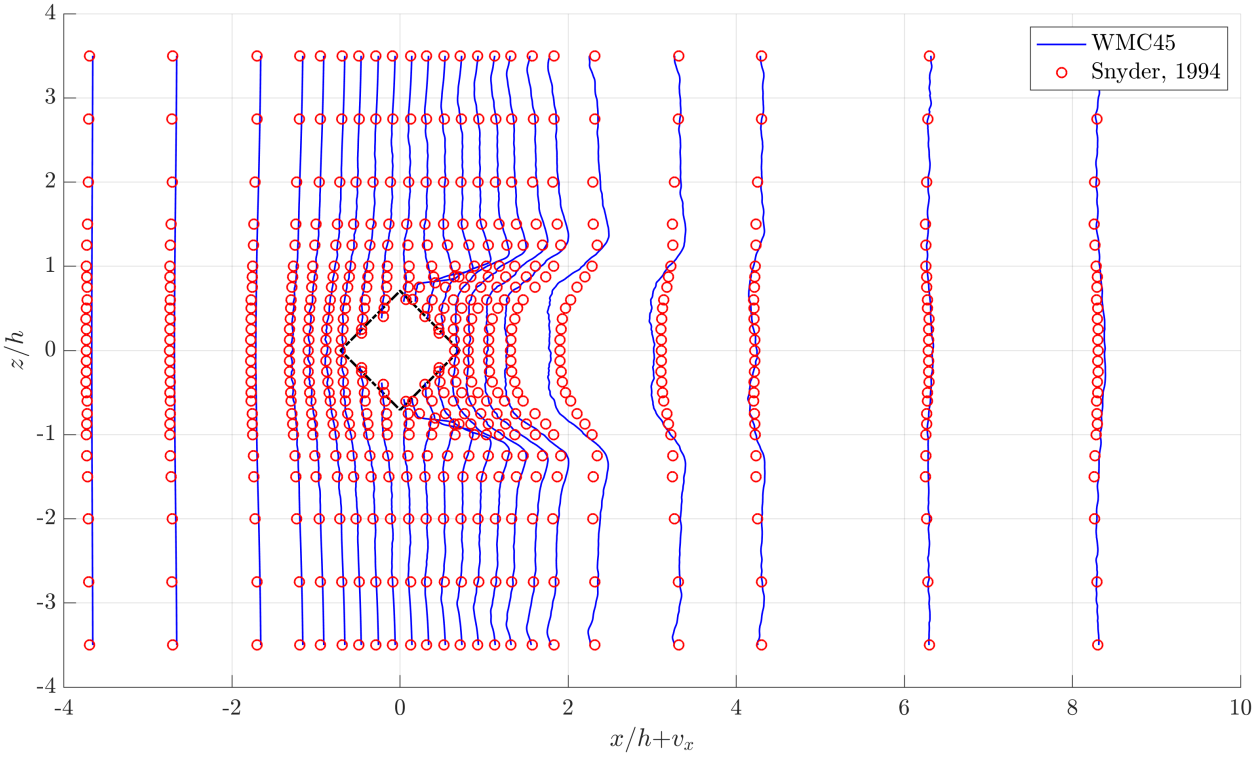

(b) Ground plane $y = 0.1h$

Figure 3: WMC45 Mean Streamwise Velocity Profiles

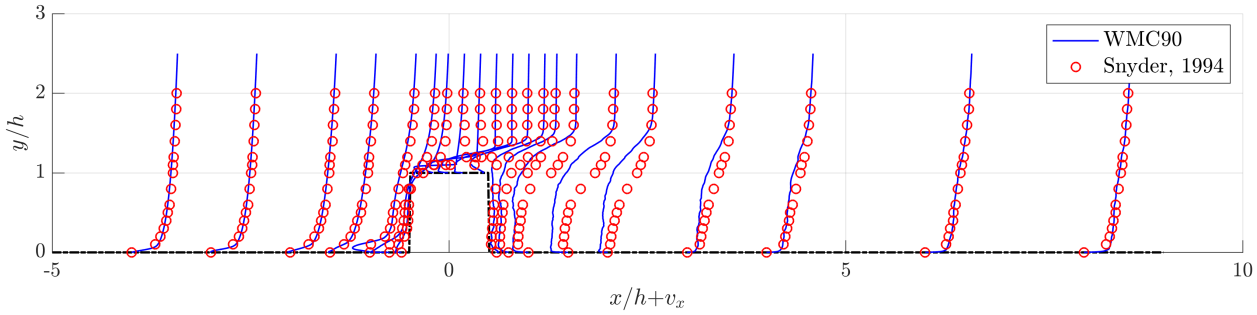

(a) Centerline plane, $z = 0$

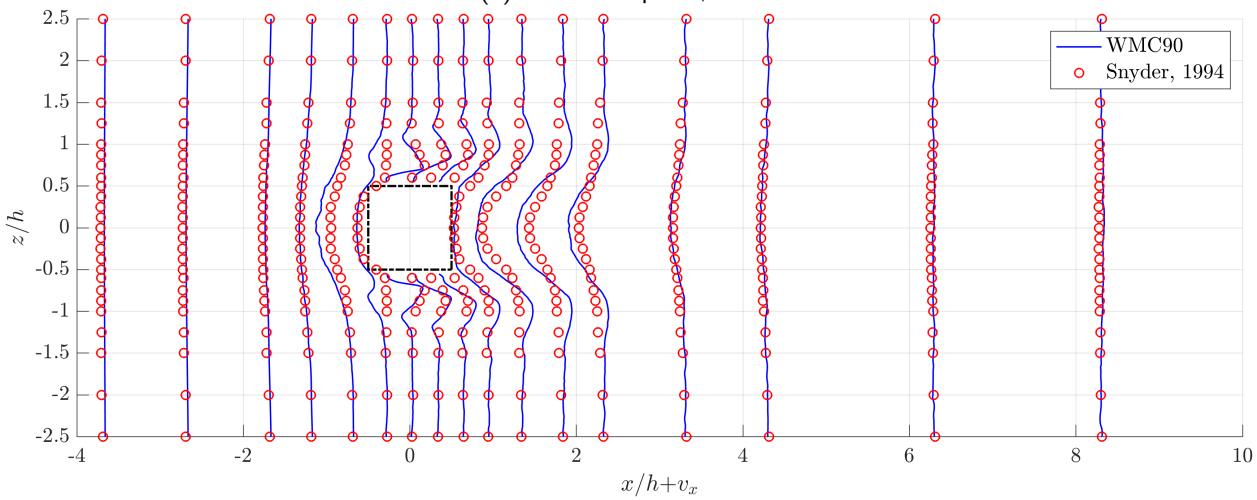

(b) Ground plane $y = 0.1h$

Figure 4: WMC90 Mean Streamwise Velocity Profiles

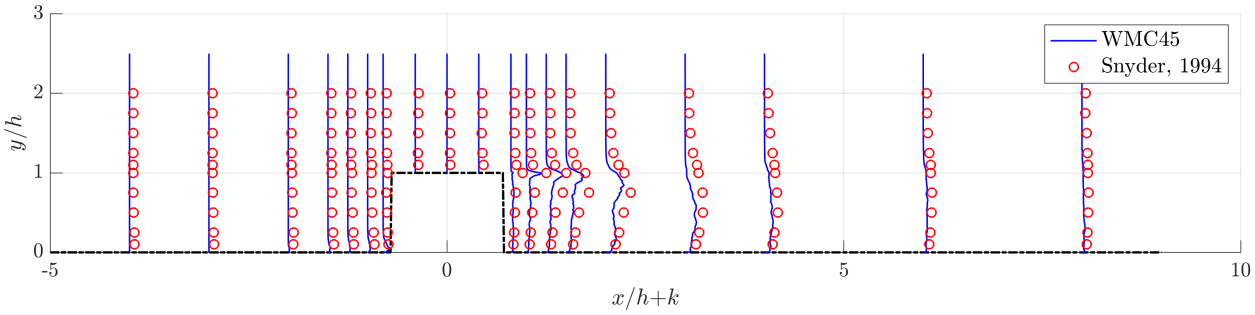

(a) Centerline plane, $z = 0$

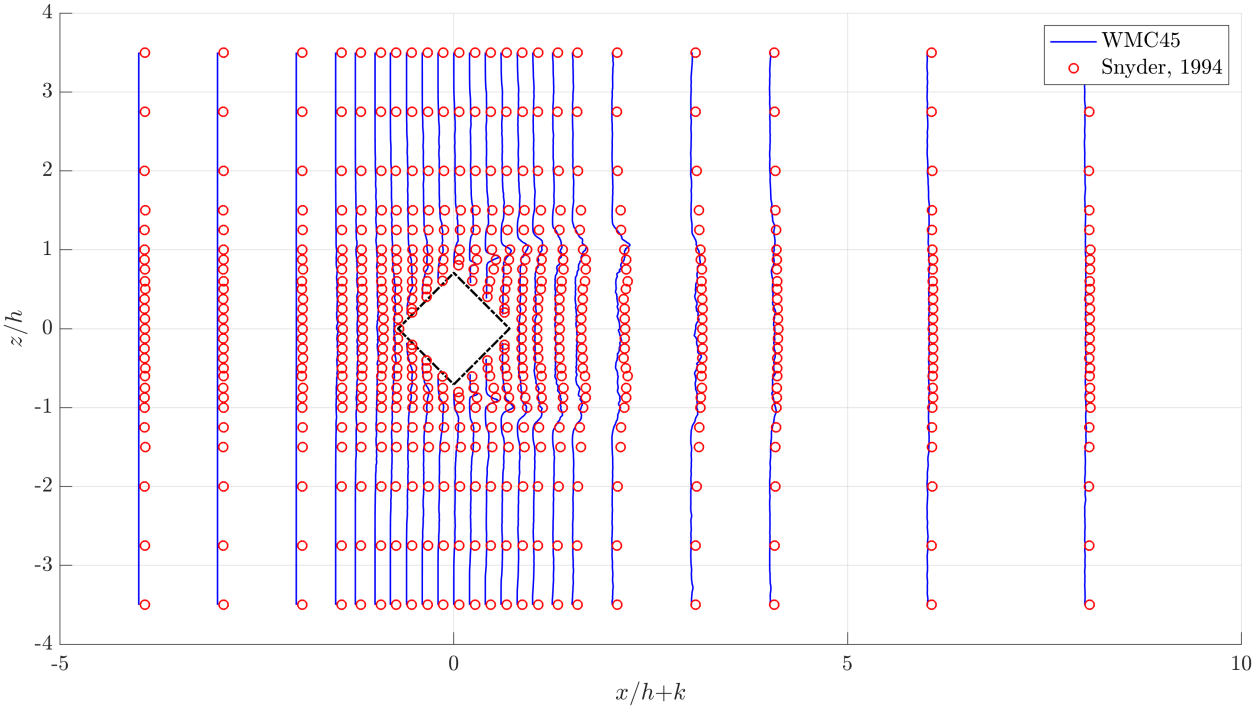

(b) Ground plane $y = 0.1h$

Figure 5: WMC45 Turbulent Kinetic Energy Profiles

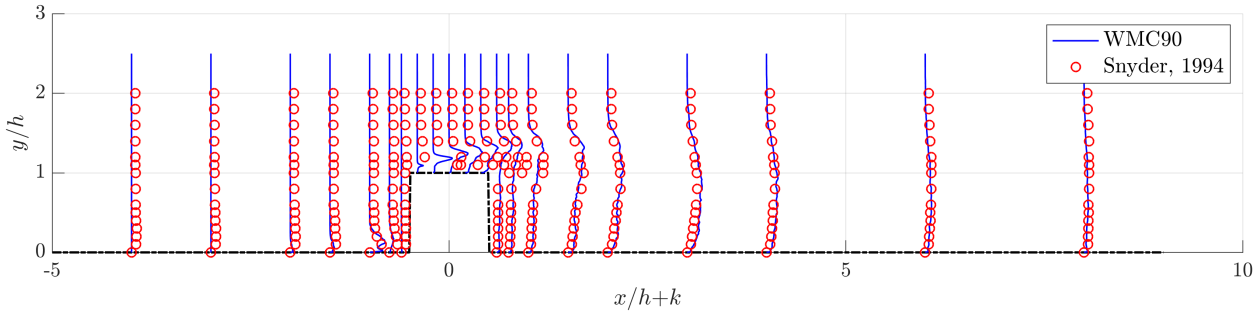

(a) Centerline plane, $z = 0$

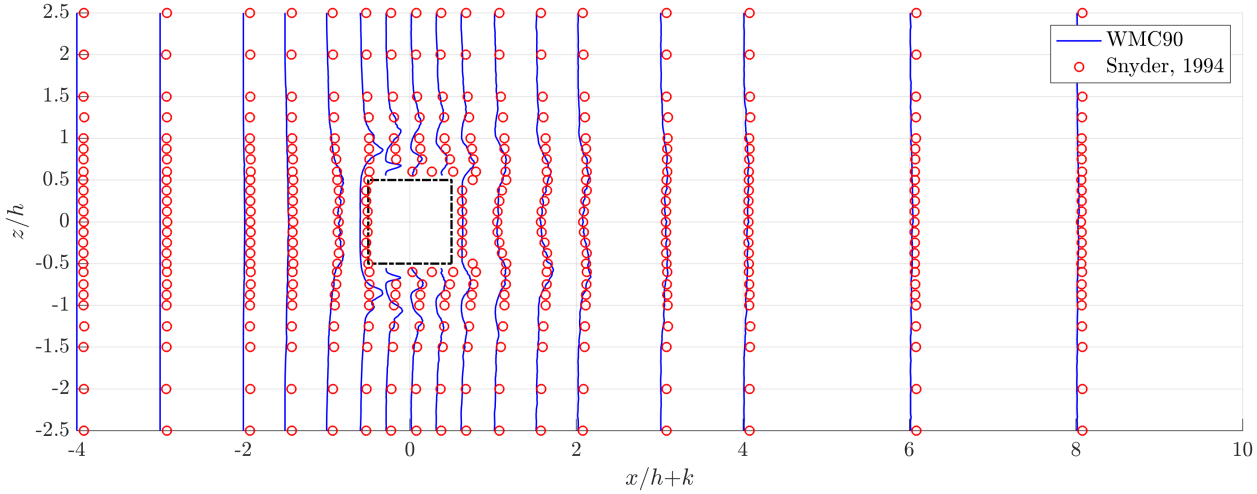

(b) Ground plane $y = 0.1h$

Figure 6: WMC90 Turbulent Kinetic Energy Profiles

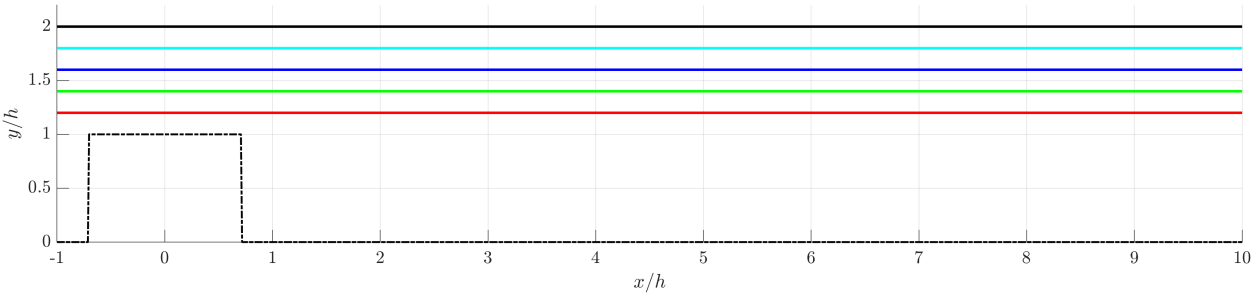

(a) Transect Locations

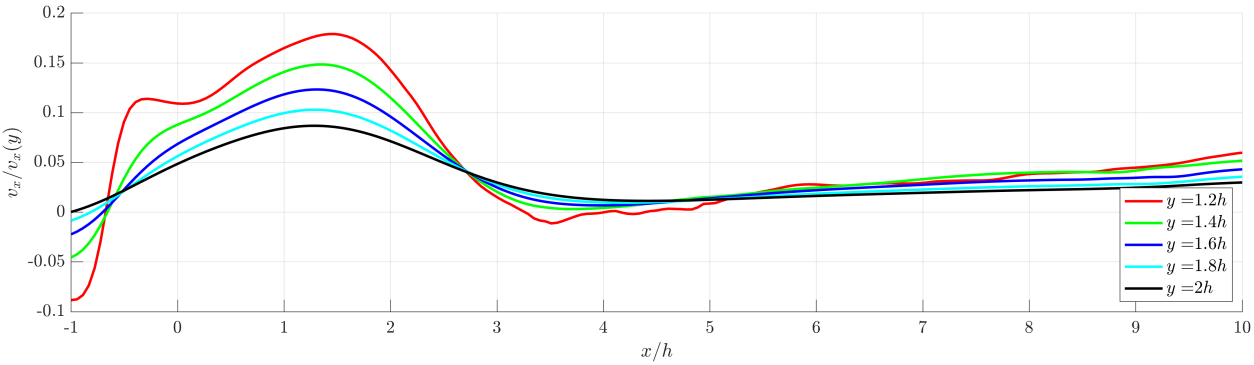

(b) Velocity Deficit

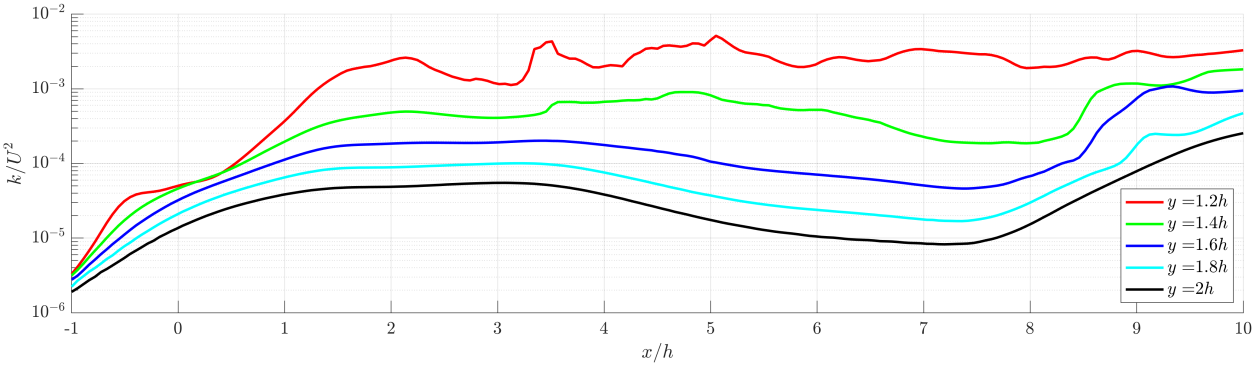

(c) Turbulent Kinetic Energy

Figure 7: WMC45 Streamwise Transects on Centerline Plane

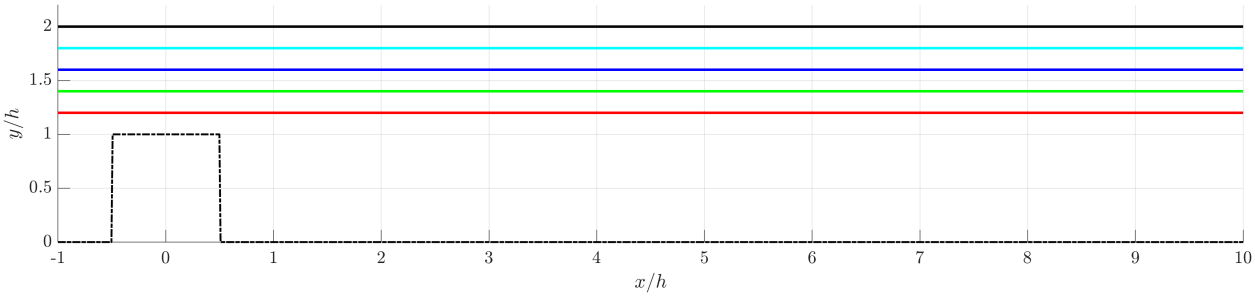

(a) Transect Locations

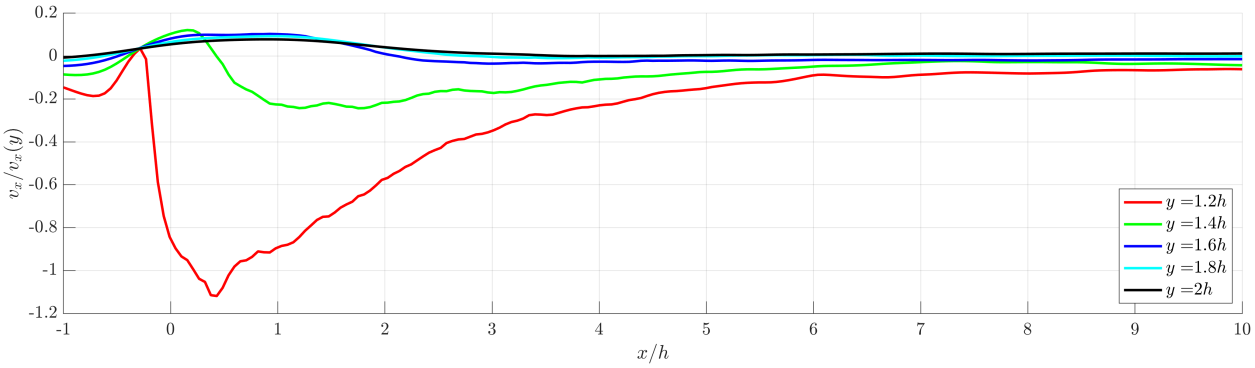

(b) Velocity Deficit

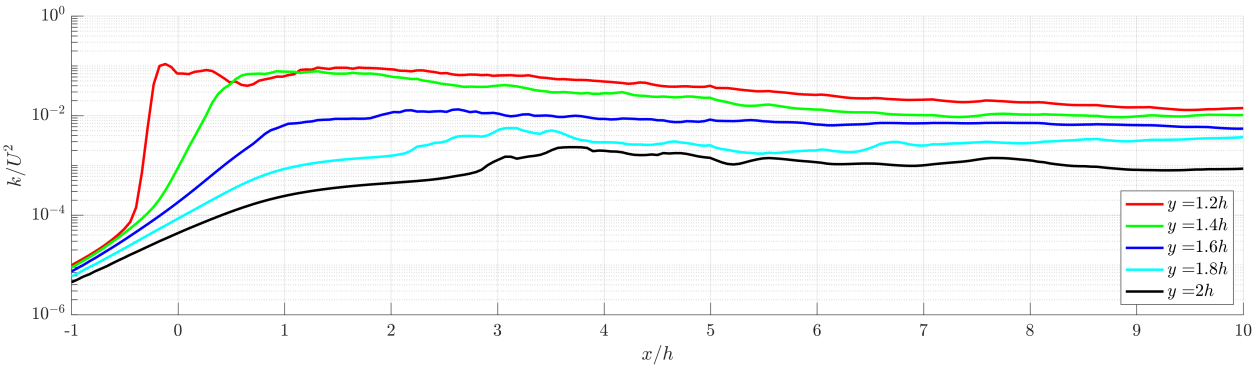

(c) Turbulent Kinetic Energy

Figure 8: WMC90 Streamwise Transects on Centerline Plane

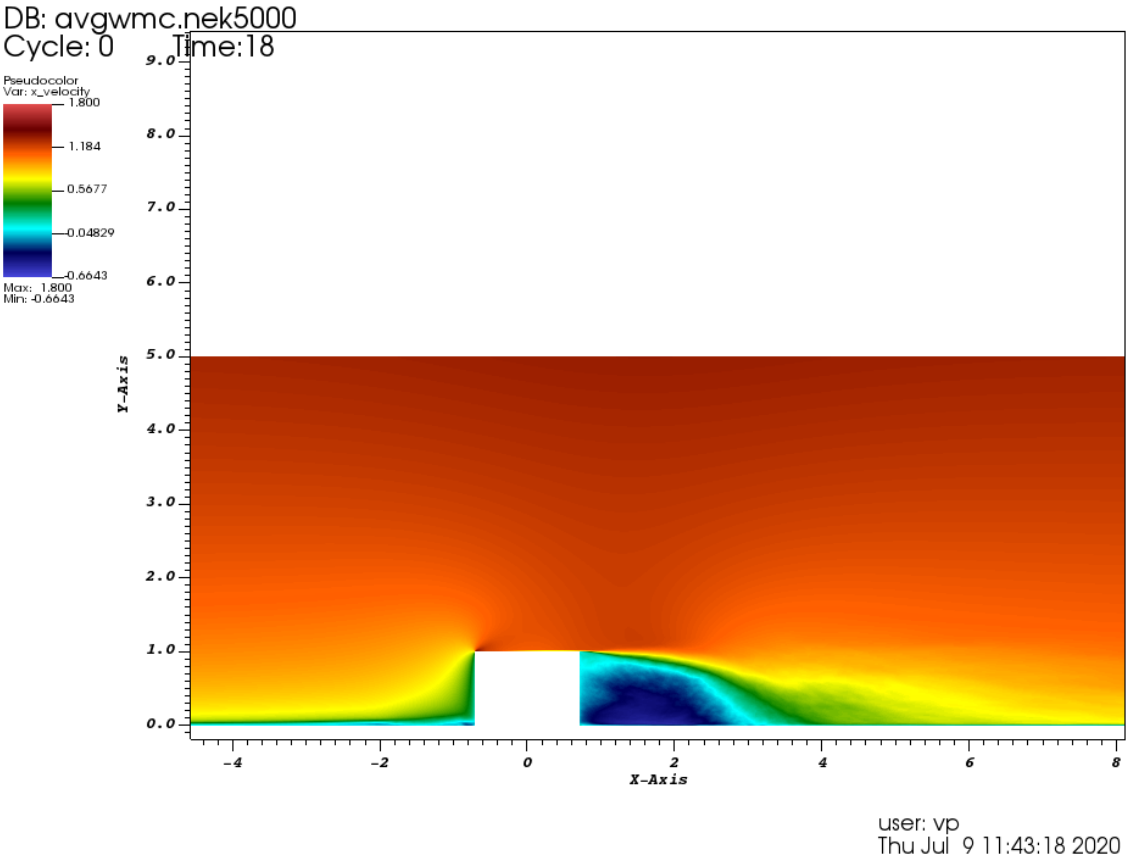

Figure 9: WMC45 v_x on centerline plane $z = 0$

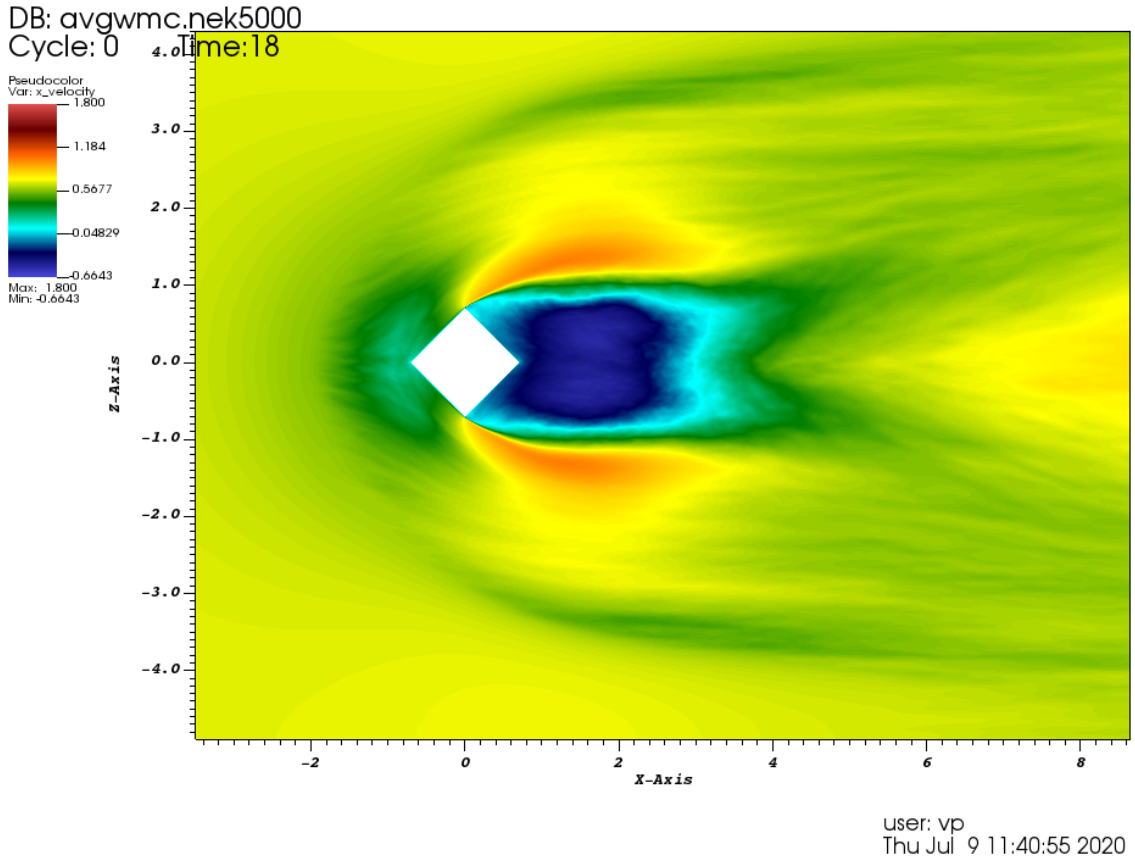

Figure 10: WMC45 v_x on ground plane $y = 0.1$

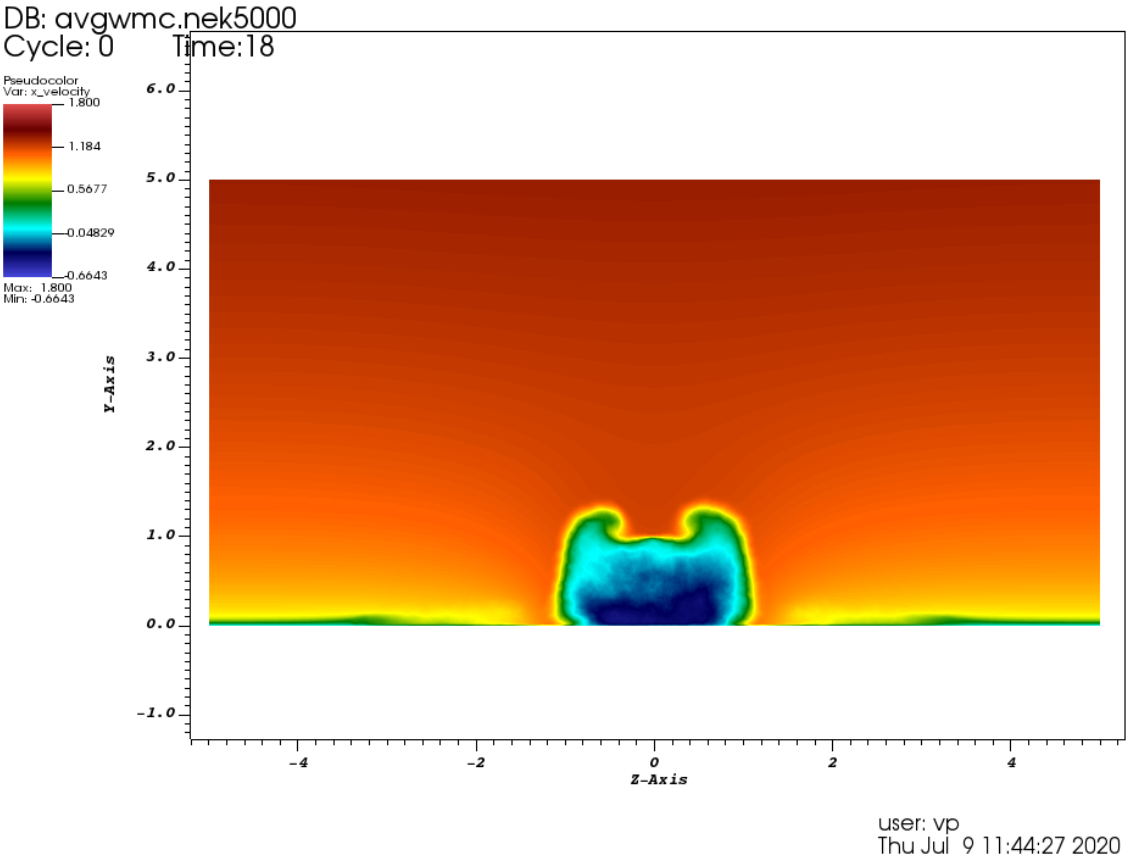

Figure 11: WMC45 v_x on plane $x = 1$

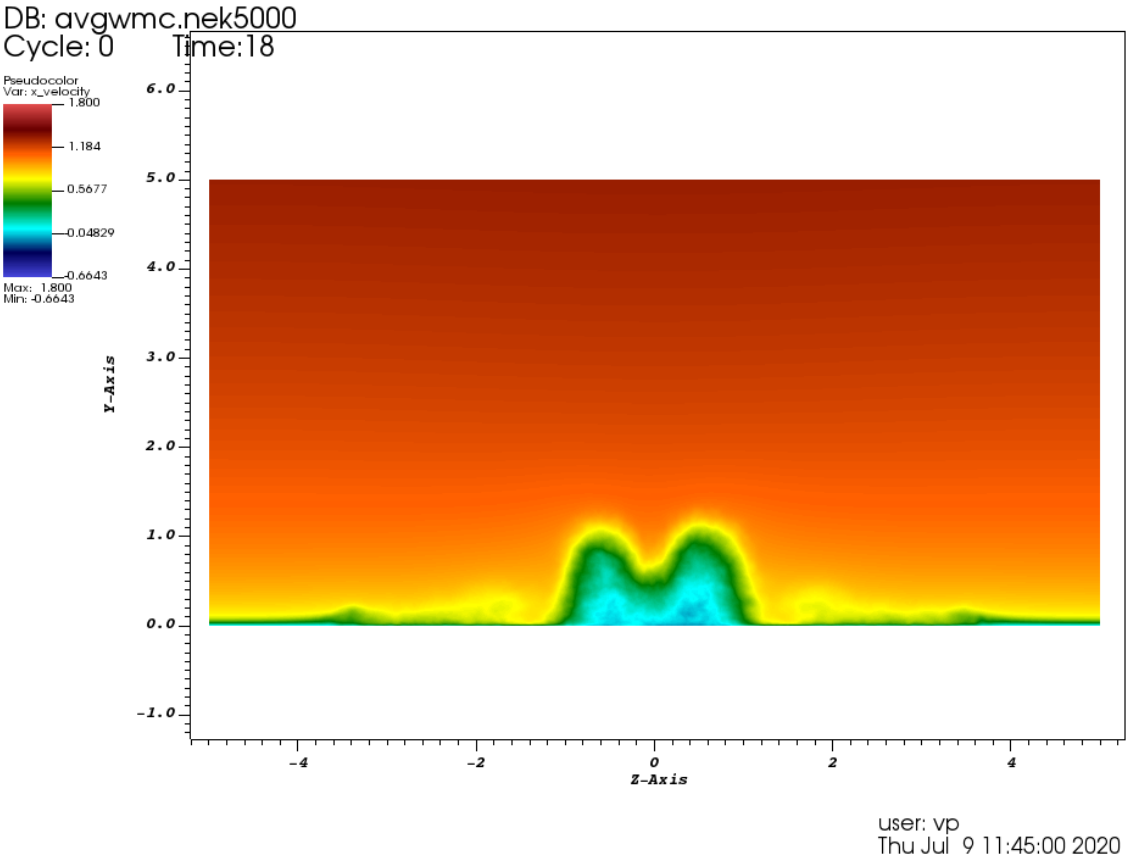

Figure 12: WMC45 v_x on plane $x = 3$

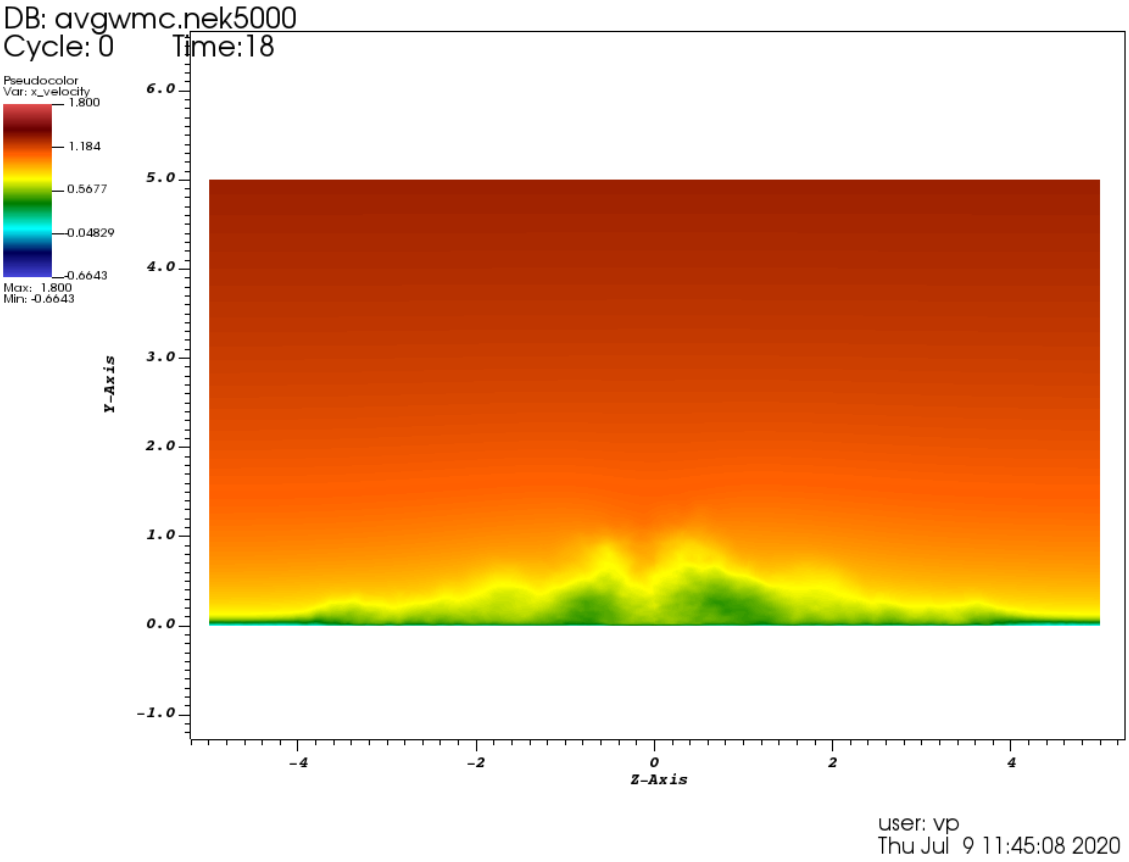

Figure 13: WMC45 v_x on plane $x = 5$

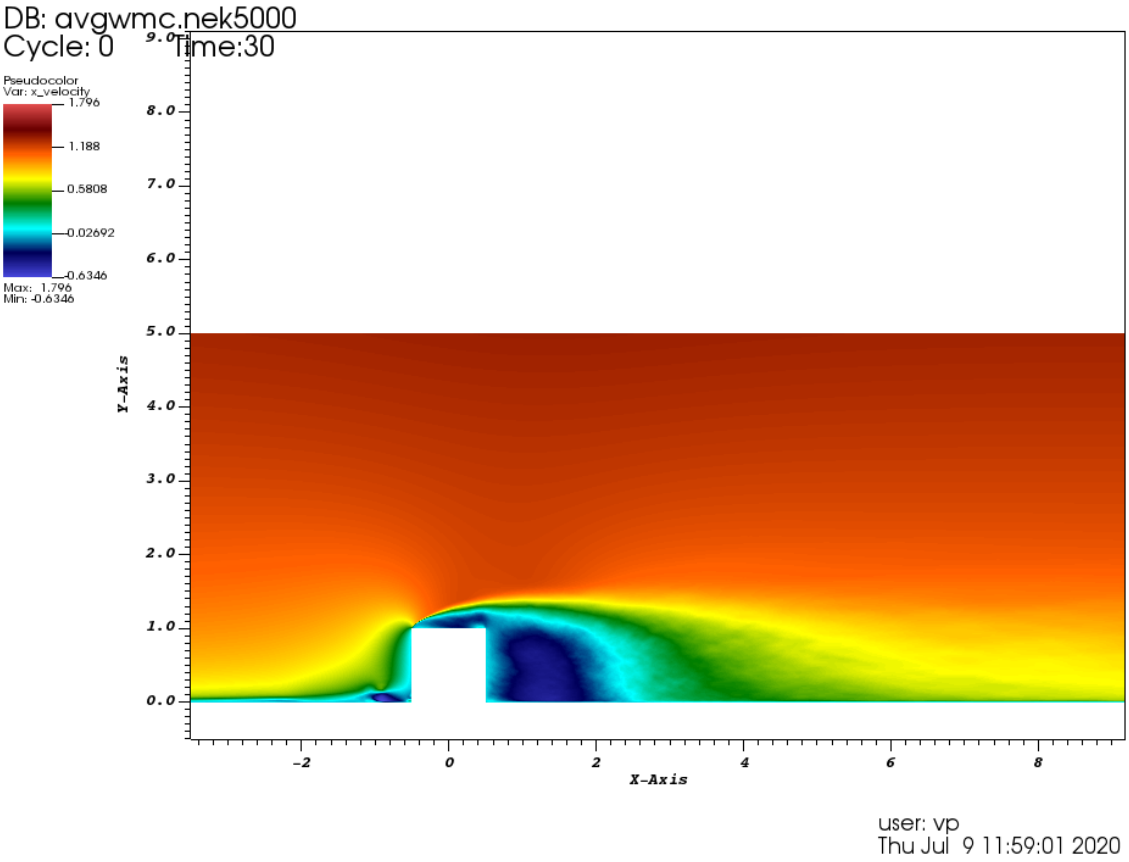

Figure 14: wmc90 v_x on centerline plane $z = 0$

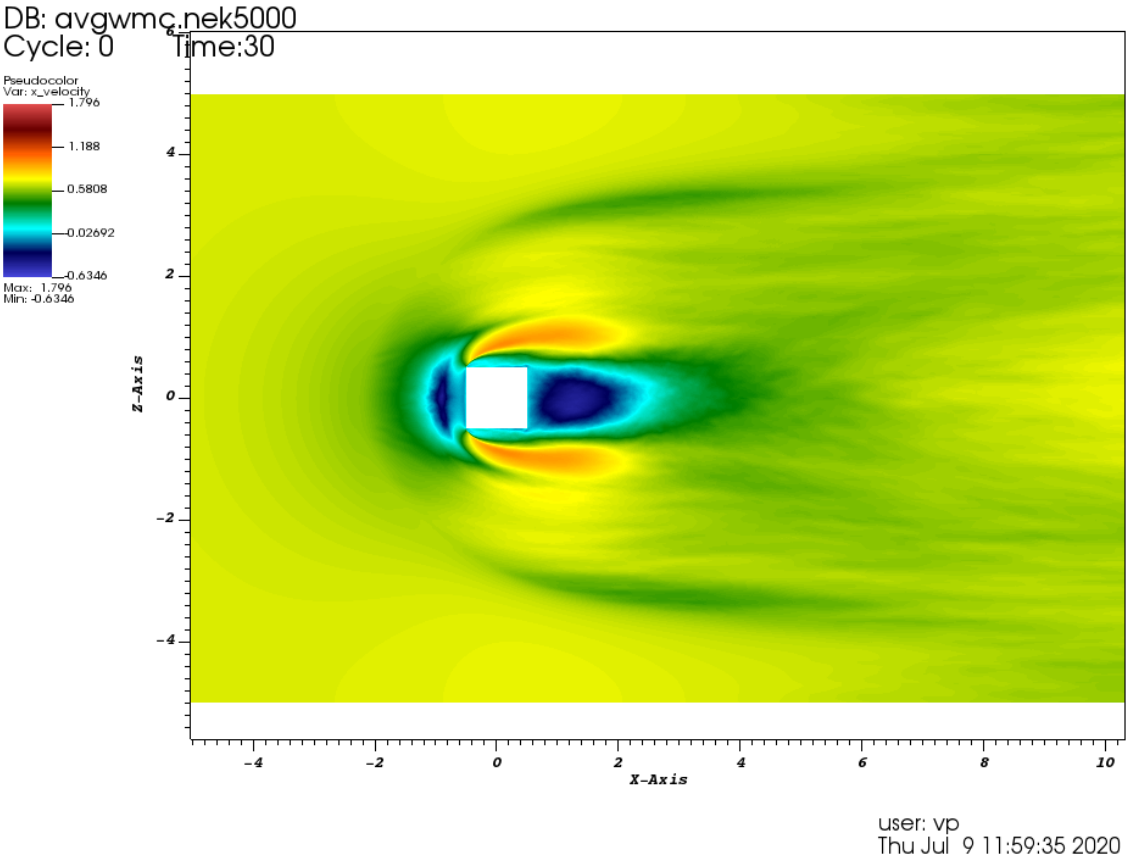

Figure 15: wmc90 v_x on ground plane $y = 0.1$

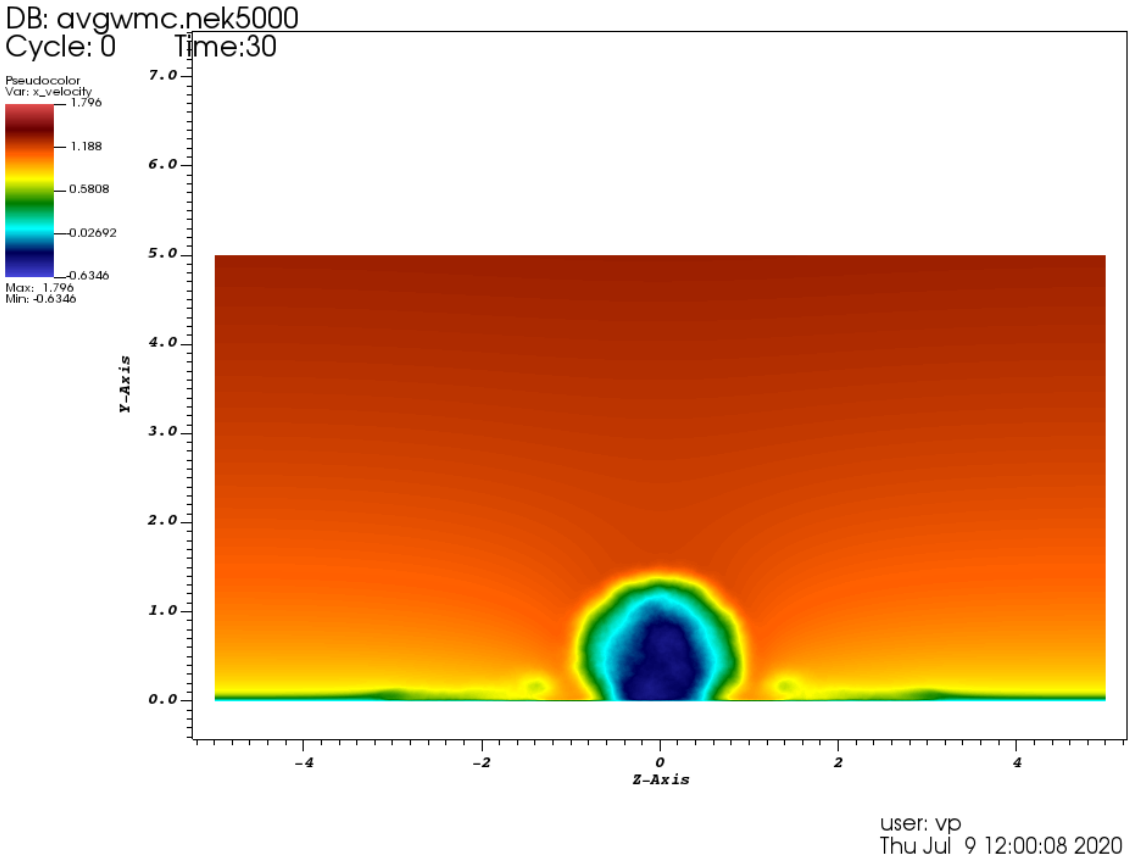

Figure 16: wmc90 v_x on plane $x = 1$

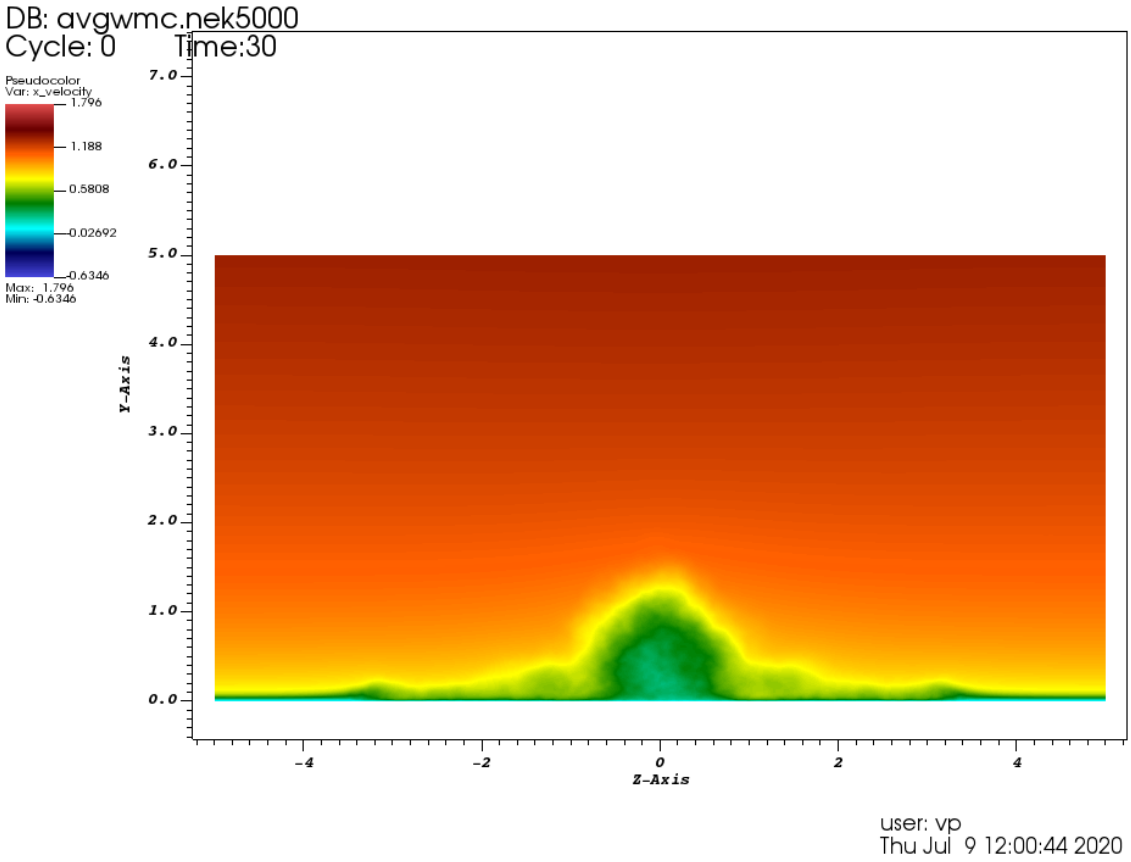

Figure 17: wmc90 v_x on plane $x = 3$

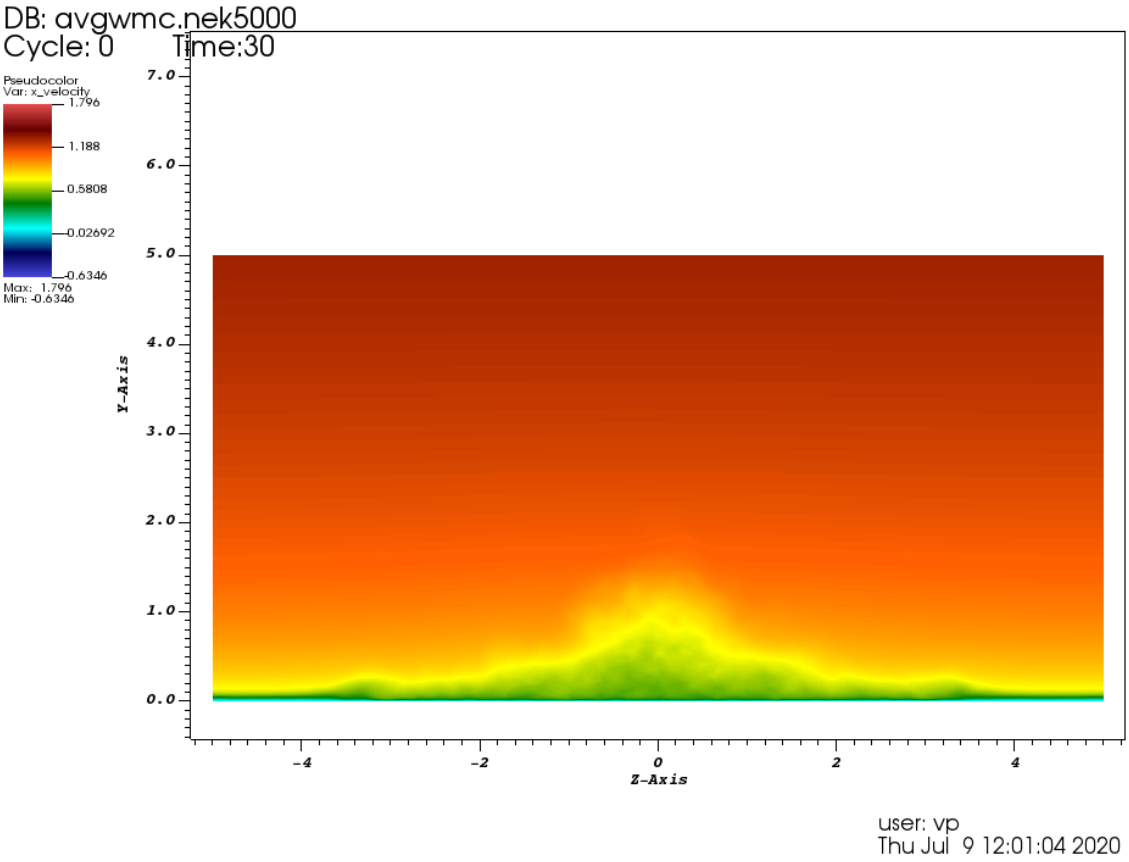

Figure 18: wmc90 v_x on plane $x = 5$